

Article

Multifactorial Modeling Reveals a Dominant Role of Wnt Signaling in Lineage Commitment of Human Pluripotent Stem Cells

Tiago P. Dias ^{1,2} , Tiago G. Fernandes ^{1,2}, Maria Margarida Diogo ^{1,2}
and Joaquim M. S. Cabral ^{1,2,*}

¹ iBB—Institute for Bioengineering and Biosciences and Department of Bioengineering, Instituto Superior Técnico, Universidade de Lisboa, Av. Rovisco Pais, 1049-001 Lisbon, Portugal

² The Discoveries Centre for Regenerative and Precision Medicine, Lisbon Campus, Instituto Superior Técnico, Universidade de Lisboa, Av. Rovisco Pais, 1049-001 Lisbon, Portugal

* Correspondence: joaquim.cabral@tecnico.ulisboa.pt

Received: 5 July 2019; Accepted: 13 August 2019; Published: 15 August 2019



Abstract: The human primed pluripotent state is maintained by a complex balance of several signaling pathways governing pluripotency maintenance and commitment. Here, we explore a multiparameter approach using a full factorial design and a simple well-defined culture system to assess individual and synergistic contributions of Wnt, FGF and TGF β signaling to pluripotency and lineage specification of human induced pluripotent stem cells (hiPSC). Hierarchical clustering and quadratic models highlighted a dominant effect of Wnt signaling over FGF and TGF β signaling, drawing hiPSCs towards mesendoderm lineages. In addition, a synergistic effect between Wnt signaling and FGF was observed to have a negative contribution to pluripotency maintenance and a positive contribution to ectoderm and mesoderm commitment. Furthermore, FGF and TGF β signaling only contributed significantly for negative ectoderm scores, suggesting that the effect of both factors for pluripotency maintenance resides in a balance of inhibitory signals instead of proactive stimulation of hiPSC pluripotency. Overall, our dry-signaling multiparameter modeling approach can contribute to elucidate individual and synergistic inputs, providing an additional degree of comprehension of the complex regulatory mechanisms of human pluripotency and commitment.

Keywords: multiparameter; factorial design; Wnt signaling; TGF β signaling; FGF signaling; human induced pluripotent stem cells; pluripotency and commitment

1. Introduction

Human induced pluripotent stem cells (hiPSCs) have an incredible potential for regenerative medicine therapies, drug-screening and disease modeling [1–3]. Understanding pluripotency and controlling commitment is essential to take full advantage of hiPSC properties and to develop efficient protocols to induce hiPSC direct differentiation into the cell types of interest.

Human pluripotency is usually associated with a primed state, controlled by a complex balance between multiple signaling pathways that govern pluripotency maintenance and exit from pluripotency towards differentiation [4–6]. This state has been connected with a weak stability and a bias towards commitment resembling the mouse epiblast state [7,8], contrasting with the increased stability of the naïve pluripotent state [9–11].

FGF, TGF β and Wnt signaling pathways are among the most important pathways controlling hiPSC fate [4–6]. These signaling pathways can be associated with pleiotropic effects, stimulating divergent cellular responses such as self-renewal and commitment [12–14]. For example, the combined

effects of FGF signaling and TGF β signaling are typically associated with hiPSCs self-renewal [4,15]. Individually, however, FGF signaling has been connected with both neuroectoderm inhibition [16] and activation [7–9]. On the other hand, TGF β signaling results in SMAD2/3 activation, which is associated with mesendoderm lineage specification [17,18]. Importantly, Wnt/ β -catenin signaling is associated with self-renewal in hiPSCs [4,19–21], in line with being essential to promote the naïve pluripotency state and inhibit epiblast transition [10,11,22,23]. However, during differentiation, Wnt signaling is also associated to self-renewal disruption and guidance of cells towards mesendoderm commitment [24,25]. Also noteworthy is the fact that Wnt signaling has a role in directing cells from neuroectoderm towards neural crest specification [25,26], and that it inhibits cardiac mesoderm specification [27,28] while promoting the epicardial cell fate [29]. Furthermore, these signaling pathways can be interconnected and influenced by multiple signals at different pathway nodes, resulting in synergistic or antagonistic effects that can shift commitment towards specific lineages [30–33]. Thus, complex and undefined culture systems with multiple signaling inputs, often using conditioned media or serum, can provide a signaling overload, contributing to divergent and pleiotropic responses, that can mask the true impact of each signaling input. Development of a multiparameter approach with a controlled signaling environment can allow to fully discern the multiple singular and cooperative contributions of each signaling input allowing the identification of synergistic and antagonistic effects [34].

We previously used a multifactorial analysis approach that revealed a significant contribution of Wnt signaling to mESC pluripotency under physiological oxygen tensions [34]. Here, we use a dry-signaling multiparameter approach consisting of a full factorial design, combining the activation of Wnt, FGF and TGF β signaling in hiPSCs cultured in a simple and well-defined culture system. Hierarchical clustering and quadratic models for human pluripotency and lineage commitment were designed and highlighted a Wnt signaling dominance with or without the presence of FGF and TGF β inputs. Synergistic effects were observed between Wnt and FGF signaling by the pluripotency, ectoderm and mesoderm models. In addition, FGF and TGF β signaling contributed negatively to the ectoderm model without a significant contribution for the pluripotency model, suggesting that a balanced inhibitory effect is promoting hiPSC pluripotency maintenance.

2. Materials and Methods

2.1. Human Induced Pluripotent Stem Cell Culture

In this work, the hiPSC cell line iPS-DF6-9-9T.B, purchased from WiCell Bank, was mainly used. This cell line is vector free and was derived from foreskin fibroblasts with a karyotype 46, XY. Both the hiPSC cell line F002.1A.13 provided by TCLab (Tecnologias Celulares para Aplicação Médica, Unipessoal, Lda.) that was generated using a retroviral system and the hiPSC line Gibco™ (Thermo Fisher Scientific, Waltham, MA, USA) derived from CD34⁺ cells of healthy donors were used to validate results as described in the different sections and figure legends.

Maintenance of hiPSC culture was performed using an mTeSR1 medium (STEMCELL Technologies, Vancouver, BC, Canada) in 6-well tissue culture plates coated with Matrigel (BD Biosciences, San Jose, CA, USA) and diluted 1:30 in DMEM/F12. The medium was changed daily. Human iPSC passaging was performed using an EDTA (Thermo Fisher Scientific, Waltham, MA, USA) solution diluted in PBS at a concentration of 0.5 mM. Cells were incubated for 5 min with EDTA at room temperature and flushed with culture medium. For maintenance cultures, splits from 1:3 to 1:8 were usually performed. For cell counting, a sample of 100 μ L was incubated in 400 μ L of Accutase for 7 min at room temperature and samples were diluted 1:2 in Trypan Blue (Thermo Fisher Scientific, Waltham, MA, USA) for counting using a hemocytometer. Culture photos were obtained using a Leica DMI 3000B microscope (Leica Microsystems GmbH, Wetzlar, Germany) and a digital camera Nikon DXM 1200 (Nikon, Tokyo, Japan).

2.2. Full Factorial Design

A 3³ full factorial design consisting of 27 culture conditions, corresponding to different concentrations of three different soluble factor activators of FGF, TGF β and Wnt signaling (FGF2, TGF β and CHIR, respectively), as well as three concentration levels (0, 1/3 and 1), was performed using E6 medium (Thermo Fisher Scientific, Waltham, MA, USA) as the basal medium. FGF2 (PeproTech, Rocky Hill, NJ, USA) concentration levels ranged from 0, 35 ng/mL to 100 ng/mL; TGF β 1 (PeproTech, Rocky Hill, NJ, USA) concentration levels ranged from 0, 0.7 ng/mL to 2 ng/mL; and CHIR99021 (Stemgent, Cambridge, MA, USA) concentration levels ranged from 0, 2 μ M to 6 μ M (Table 1). Three blocks of 9 culture conditions (samples) were performed each time with mTeSR1, E8 and E6 as controls. Cells were collected by EDTA Enzyme-free passaging and were seeded at 37,500 cells/cm² using an mTeSR1 medium, to guarantee that the results of the study would not be affected by cell confluence. Conditions were exposed to the respective cocktail after 24 h and fresh supplemented medium changed every 24 h for 4 consecutive days of exposure. Fresh medium was prepared every day and supplemented with the cytokines and small molecules prior to medium change. After 4 days of exposure, cells were singularized using Accutase for 7 min, centrifuged, and a sample counted to evaluate cell number fold increase (FI) using trypan blue. Cells were washed with PBS, centrifuged, and the cell pellets were stored at -80° C to perform real-time PCR afterwards.

Table 1. Full factorial design conditions. FGF2 concentration levels ranged between 0, 35, and 100 ng/mL; TGF β concentration levels ranged between 0, 0.85, and 2 ng/mL; and CHIR concentration levels ranged between 0, 2, and 6 μ M.

Samples	FGF2 (ng/mL)	TGF β (ng/mL)	CHIR (μ M)
Sample 1/E6	0	0	0
Sample 2	0	0	2
Sample 3	0	0	6
Sample 4	0	0.7	0
Sample 5	0	0.7	2
Sample 6	0	0.7	6
Sample 7	0	2	0
Sample 8	0	2	2
Sample 9	0	2	6
Sample 10	35	0	0
Sample 11	35	0	2
Sample 12	35	0	6
Sample 13	35	0.7	0
Sample 14	35	0.7	2
Sample 15	35	0.7	6
Sample 16	35	2	0
Sample 17	35	2	2
Sample 18	35	2	6
Sample 19	100	0	0
Sample 20	100	0	2
Sample 21	100	0	6
Sample 22	100	0.7	0
Sample 23	100	0.7	2
Sample 24	100	0.7	6
Sample 25	100	2	0
Sample 26	100	2	2
Sample 27	100	2	6

2.3. Human iPSC-Cardiomyocyte (hiPSC-CM) Differentiation

Human iPSCs were seeded at a density of 1×10^5 cells/cm² and maintained in pluripotency conditions with daily medium changes. When confluence reached percentages around 95%, hiPSC cardiac differentiation was induced following the Wnt signaling modulation protocol previously described by Lian et al. [35]. Experiments were performed using 1 μ M or 6 μ M of the GSK3 β inhibitor CHIR99021

(Stemgent, Cambridge, MA, USA) at day 0 and with or without 5 μM of the Wnt signaling inhibitor IWP4 (Stemgent, Cambridge, MA, USA) at day 3. Cells were collected and analyzed at day 15 of differentiation.

2.4. Human iPSC-Neural Differentiation

Human iPSCs were seeded at a density of 2×10^5 cells/cm² using E8. For E6 differentiation, after overnight growth, the medium was changed to E6 as previously described by Lippmann et al. [36]. For dual SMAD Inhibition-based neural induction, after cultures were nearly confluent, the medium was changed to 1:1 N2/B27 media supplemented with 10 μM SB431542 (Stemgent, Cambridge, MA, USA) and 100 nM LDN193189 (Stemgent, Cambridge, MA, USA), as previously described [37,38]. For both protocols, the medium was changed daily, and cells were collected and analyzed at day 12 of differentiation.

2.5. Flow Cytometry

Cells were washed with PBS, singularized and fixed using 2% (*v/v*) PFA for 20 min at room temperature. Cells were centrifuged and resuspended in 90% (*v/v*) cold methanol, incubated for 15 min at 4 °C. Samples were then washed 3 times using a solution of 0.5% (*v/v*) BSA in PBS (FB1). Primary antibody Cardiac Troponin T (CTNT) monoclonal mouse IgG antibody (Thermo Fisher Scientific, Waltham, MA, USA, Clone 13-11, dilution 1:250) or Primary antibody T/Brachyury polyclonal goat IgG antibody (R&D Systems, dilution 1:20) were diluted in FB1 plus 0.1% (*v/v*) Triton (FB2) and incubated for 1 h at room temperature. Cells were then washed and the cell pellet resuspended with the secondary antibody goat anti-mouse Alexa-488 (Thermo Fisher Scientific, Waltham, MA, USA) for CTNT or secondary antibody donkey anti-goat Alexa-488 for T/Brachyury (Thermo Fisher Scientific, Waltham, MA, USA), both diluted 1:1000 in FB2 and incubated for 30 min in the dark. Finally, cells were washed twice and cell pellets were resuspended in 500 μL of PBS and analyzed in a FACSCalibur flow cytometer (Becton Dickinson, Franklin Lakes, NJ, USA). Data were analyzed using the software “Flowing Software” at <http://www.flowingsoftware.com> (version 2.5).

2.6. Immunofluorescence Staining

Cells were fixed with 4% (*v/v*) PFA for 15 min, washed with PBS and incubated with blocking solution (10% *v/v* NGS, 0.1% *v/v* Triton-X in PBS) for 1 h. After incubation, for hiPSC-CM differentiation, Cardiac Troponin T (CTNT) monoclonal mouse IgG antibody (Thermo Fisher Scientific, Waltham, MA, USA, Clone 13-11) was diluted 1:250 in staining solution (5% *v/v* NGS, 0.1% *v/v* Triton-X in PBS) and incubated for 2 h at room temperature. For hiPSC-Neural commitment, NESTIN monoclonal mouse IgG antibody (R&D Systems, Minneapolis, MN, USA) and PAX6 polyclonal rabbit IgG antibody (Covance, Princeton, NJ, USA) were used both diluted 1:1000 in staining solution and incubated for 2 h at room temperature. After washing with PBS, secondary antibodies goat anti-mouse IgG Alexa-546 and goat anti-rabbit IgG Alexa-488 (Thermo Fisher Scientific, Waltham, MA, USA) were diluted 1:500 in staining solution and incubated for 1 h at room temperature. Samples were then washed 2 times with PBS, incubated for 2 min with 3 $\mu\text{g}/\text{mL}$ of DAPI diluted in PBS, washed again 3 times, and stored at 4 °C. Samples were analyzed using a fluorescence optical microscope (Leica DMI 3000B, Leica Microsystems GmbH, Wetzlar, Germany) and a digital camera (Nikon DXM 1200, Nikon, Tokyo, Japan). Images were processed using ImageJ/Fiji (<http://fiji.sc>) [39] and PAX6⁺ cells were quantified using CellProfiler (Broad Institute, Cambridge, MA, USA).

2.7. Real-Time PCR

RNA from each condition and controls was extracted using the High Pure RNA Isolation Kit (Roche, Basel, Switzerland) following the instructions provided with the Kit. RNA was quantified using a nanodrop, and 1 μg of RNA was converted to cDNA using the High Capacity cDNA Reverse Transcription Kit (Thermo Fisher Scientific, Waltham, MA, USA) following the instructions provided with the kit. Relative gene expression was evaluated using 10 ng of cDNA, 250 μM of each primer (Table S1) and using the Fast SYBR Green Master Mix (Thermo Fisher Scientific, Waltham, MA, USA)

with an annealing temperature set to 60 °C. Melting curves were performed at the end to assess if primers were amplifying only the correct amplicon. Values were treated following the $2^{-\Delta\Delta CT}$ method. *GAPDH* gene expression was used as endogenous control and relative expression was calibrated for each gene using mTeSR1 gene expression values. For hiPSC-CM differentiation, relative expression was calibrated using day 0 of differentiation.

For hiPSC-Neural commitment, real-time PCR was performed using the TaqMan Gene Expression Assay (Thermo Fisher Scientific, Waltham, MA, USA) for the genes *OCT4/POU5F1* (Hs00999634_gH), *NANOG* (Hs02387400_g1), *PAX6* (Hs00240871_m1), *SOX1* (Hs01057642_s1) and *GAPDH* (Hs02758991_g1). *GAPDH* gene expression was used as endogenous control and relative expression was calibrated using day 0 of differentiation.

2.8. Panels and Scores

Relative expression values were normalized using the minimum and maximum value obtained for each gene. Then, panels for pluripotency (*OCT4* and *NANOG*), ectoderm (*FGF5*, *PAX6* and *P75*), mesendoderm (*MIXL1* and *T*), mesoderm (*NKX2.5* and *MESP1*) and endoderm (*SOX17* and *PDX1*) were created by averaging the expression value of each gene. Then, scores for pluripotency and for each lineage were empirically calculated as follows:

$$\text{Pluripotency Score} = 1.5 \times \text{Pluripotent Panel} - 0.25 \times \text{Ectoderm Panel} - 0.25 \times \text{Mesendoderm Panel} - 0.5 \times \text{Mesoderm Panel} - 0.5 \times \text{Endoderm Panel}, \quad (1)$$

$$\text{Ectoderm Score} = 1.75 \times \text{Ectoderm Panel} - 0.25 \times \text{Pluripotent Panel} - 0.5 \times \text{Mesendoderm Panel} - 0.5 \times \text{Mesoderm Panel} - 0.5 \times \text{Endoderm Panel}, \quad (2)$$

$$\text{Mesendoderm Score} = \text{Mesendoderm Panel} + 0.25 \times \text{Endoderm Panel} + 0.25 \times \text{Mesoderm Panel} - 0.5 \times \text{Ectoderm Panel} - \text{Pluripotent Panel}, \quad (3)$$

$$\text{Endoderm Score} = 2 \times \text{Endoderm Panel} + 0.5 \times \text{Mesendoderm Panel} - 0.5 \times \text{Mesoderm Panel} - \text{Ectoderm Panel} - \text{Pluripotent Panel}, \quad (4)$$

$$\text{Mesoderm Score} = 2 \times \text{Mesoderm Panel} + 0.5 \times \text{Mesendoderm Panel} - 0.5 \times \text{Endoderm Panel} - \text{Ectoderm Panel} - \text{Pluripotent Panel}. \quad (5)$$

The main results showed in this study using scores were not changed when panels or individual gene expression were used. Nevertheless, scores helped to clarify the true effect of signal combinations, leading to more robust, statistically significant models.

2.9. Hierarchical Clustering and PCA

Hierarchical clusters and principal component analysis (PCA) were performed using Clustvis, a web tool based on R [40]. Clusters were obtained using Pearson correlation and average linkage. PCA were obtained using the Clustvis default SVD imputation.

2.10. Full Factorial Design Models and Statistical Analysis

A model for each score was created using Statistica Software. Models were obtained by fitting the data to a full quadratic model (linear, quadratic and two-way interactions) with centered and scaled polynomials, as follows:

$$Y_i = \beta_0 + \beta_1[X_1] + \beta_{11}[X_1]^2 + \beta_2[X_2] + \beta_{22}[X_2]^2 + \beta_3[X_3] + \beta_{33}[X_3]^2 + \beta_{12}[X_1][X_2] + \beta_{13}[X_1][X_3] + \beta_{23}[X_2][X_3] \quad (6)$$

where Y_i corresponds to the specific score; β_0 is the intersect coefficient; β_1 , β_2 and β_3 are the coefficients correspondent to the linear main effects; β_{11} , β_{22} and β_{33} are the quadratic coefficients and β_{12} , β_{13} and β_{23} are the coefficients for factor interactions. The full factorial design with three replicates of Sample 1 (E6) resulted in a total of 28 degrees of freedom. Statistical significance for each model was assessed by ANOVA using Fisher's statistical test, in which factors with p -values lower than 0.05 were considered

to have a statistically significant contribution to the model [34,41]. Models were not further refined by discarding non-statistically significant factors. Nevertheless, R^2 -adjusted (R^2 -Adj), a modified version of R^2 , is also showed for every model. R^2 -Adj compares the explanatory power of the regression models calculated with many prediction factors by discarding factors that do not significantly improve model prediction, and therefore helps to assess the true quality of the model.

3. Results

3.1. Full Factorial Analysis in a “Dry-signaling” Culture System

To expose the impact of FGF signaling, TGF/Nodal signaling and Wnt signaling in human pluripotency and exit towards differentiation, a full factorial design was conceived to detect dual signaling roles by combining three concentration levels of each signaling input: Zero, lower activation (1/3 of higher activation) and higher activation, using E6/VTN [15], a dry-signaling system, as the basal culture medium (Figure 1). When compared with the E8 formulation [15], the E6 medium has only insulin as a principal signaling input, eliminating from its formulation FGF2 and Nodal/TGF β . The experimental design covered 27 different conditions (Table 1). In addition, three replicates of each E6 basal media (Sample 1), mTeSR and E8 experiments were performed as controls.

In our multiparameter approach, FGF pathway was modulated using FGF2 at concentrations of 0, 35 and 100 ng/mL. Both TeSR and E8 medium use 100 ng/mL of FGF2 to maintain hiPSC pluripotency [15,42]. At this concentration and higher, a plateau of maximal activity is observed for downstream FGF signaling targets such as ERK and FRS-2 [12]. In fact, maximum activation of both downstream targets can be observed at 10 ng/mL, which can contribute to the pleiotropic behavior of FGF signaling [12]. In addition, TGF pathway was modulated using TGF β 1 at concentrations of 0, 0.7 and 2 ng/mL. E8 medium uses 1.74 ng/mL of TGF β 1 to maintain hiPSC pluripotency, although this concentration also has an impact in fibroblast proliferation and can inhibit hiPSC reprogramming [43]. In TeSR, 0.6 ng/mL of TGF β 1 has a mild contribution to maintain pluripotency by directly targeting NANOG [17,42]. TGF β 1 at a concentration of 1 ng/mL seems to be enough to plateau maximum expression of downstream targets such as SMAD3 and release of IL-6 and CXCL8 [13]. Lastly, the Wnt pathway was modulated using the small chemical inhibitor CHIR99021 (CHIR) at concentrations of 0, 2 and 6 μ M, which inhibits GSK3 β leading to canonical Wnt signaling activation [44]. CHIR is one of the most potent and specific GSK3 β inhibitors in vitro and seems to not significantly affect other kinases [44–47]. A concentration of 6 μ M of CHIR is commonly used to promote hiPSC exit from pluripotency towards mesendoderm [28,35]. Lower concentrations, usually up to 2 μ M, are found to be involved in self-renewal of human naïve PSCs [10], while 3 μ M in the presence of dual SMAD inhibitors can induce hPSC neural crest differentiation [48].

Each condition of the full factorial design was assessed by analyzing the overall fold increase in total cell numbers, colony morphology and by real-time PCR, allowing the attribution of scores to each condition and the assessment of the data by clustering and modeling tools (Figure 1B). To assess the effect of each input, human iPSCs were seeded in VTN using mTeSR1. After 24 h, hiPSCs were exposed to the respective cocktail of signaling inputs using E6 as basal media. Exposure was performed for 4 days, changing the media every 24 h, to assess if specific cocktail combinations contributed to maintain pluripotency or guided cells to differentiation. Cell fold increase for all experimental conditions (samples) was evaluated after 5 days in culture (Figure 2A). All experimental conditions promoted cell growth, although, in general, cells exposed to media cocktails without CHIR presented a lower cell growth compared to conditions with CHIR supplementation. This result was consistent with the cell morphology observed, with cells exposed to cocktails containing CHIR showing a more differentiated-like phenotype at day 4 when compared with more well-defined compact colonies, typically associated with the pluripotent state, for cells without exposure to CHIR (Figure 2B). These cell morphology changes were observed gradually with increased CHIR exposure time (Figure S1). The effect of Wnt activation in colony morphology is in clear contrast with the effect of CHIR, at lower

concentrations, commonly observed for mice or human cells in the naïve state of pluripotency with round-cells organized in a more compact and multilayer-like colony morphology [9,11,34,49].

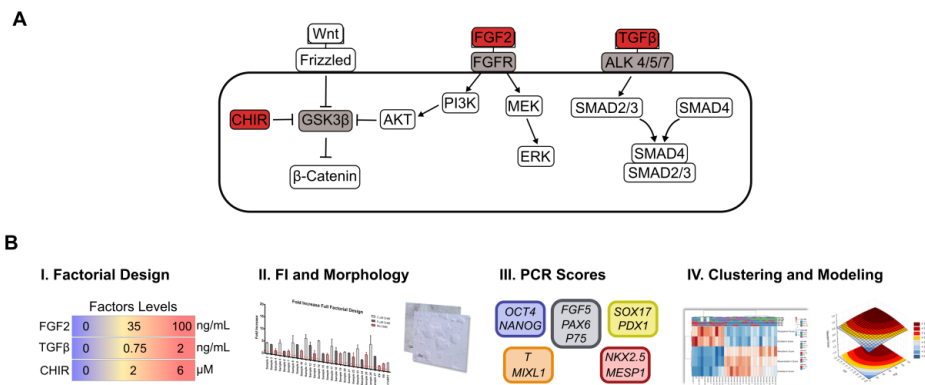


Figure 1. Schematic representation of the experimental framework used in this study. (A) A multiparameter approach was designed to reveal FGF, TGF/Nodal and Wnt signaling synergistic impact on human pluripotency and exit towards differentiation. (B) Multiparameter methodology performed. (i) A full factorial design combining 3 factors and 3 concentration levels for each factor was performed using E6 and Vitronectin as a dry-signaling culture system. Cells were exposed to the respective molecule cocktails for 4 days, with the medium changed daily. (ii) Proliferation and morphology were assessed for all 27 conditions plus mTeSR1 and E8 at the end of the 4-day culture. (iii) Real-time PCR was performed for each panel, and scores for pluripotency, ectoderm, mesendoderm, mesoderm and endoderm were calculated for each condition. Finally, (iv) scores obtained for each condition were hierarchical clustered and fitted to full quadratic models for each score.

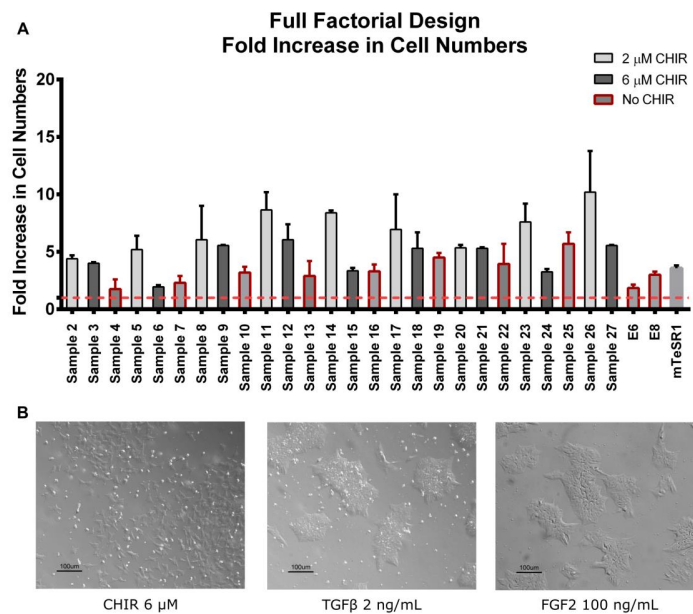


Figure 2. Human iPSC fold increase in total cell numbers and morphology of full factorial design conditions and controls. (A) Cell fold increase of all full factorial design conditions and controls. Red-dotted line marks the minimal threshold for fold increase achievement (FI = 1). In general, medium cocktails supplemented with CHIR showed higher cell fold increases when compared to cocktails without CHIR (highlighted in red). Error bars, standard error of the mean (SEM), $n = 2$. p -value < 0.01 by one-way ANOVA. (B) Typical morphology of cultures with CHIR addition compared to cultures without CHIR addition after 72 h of exposure to signaling inputs. Cultures without CHIR retained typical pluripotent colony morphology when compared to E8 or mTeSR1, while CHIR supplementation showed no colonies, which is associated with a more committed phenotype. See Table 1 for detailed concentrations of samples.

3.2. Pluripotency and Lineage Specification Evaluation Using Hierarchical Clustering and Principal Components Analysis

To assess the effect on cells exposed to each signaling input, real-time PCR was performed to analyze the expression of a set of genes (Table S1), corresponding to pluripotency and different lineage markers, whose expression levels could indicate if pluripotency was maintained or cells started to commit towards a specific lineage upon exposure to the different molecular cocktails. For the pluripotency panel, OCT4 and NANOG were selected, since both form the pluripotency core with SOX2, with OCT4 being enough to maintain and induce pluripotency [50] and NANOG being a sensible marker and gatekeeper of the pluripotent state [51–53]. Ectoderm panel was constituted by FGF5, a post-implantation primitive ectoderm marker [54]; PAX6, an early marker of neuroectodermal differentiation [55]; and P75, a neural crest cell marker [26]. Mesendoderm panel was composed by the primitive streak genes T/Brachyury, essential for primitive streak formation and mesendoderm differentiation, and MIXL1, a mesendoderm morphogen appearing at later stages of differentiation [56–58]. The endoderm panel was constituted by SOX17, a sensitive definitive endoderm marker [18,31], and PDX1, a foregut endoderm marker and regulator of pancreas specification [59]. The mesoderm panel was defined by MESP1, an early mesoderm marker that contributes to the specification of multiple mesoderm lineages in a context-dependent manner [60], and NKX2.5, a cardiac mesoderm marker expressed upon cardiac crescent formation [61].

To emphasize the main path that hiPSCs were following after exposure to the signaling cocktails, scores to each lineage commitment and pluripotency were attributed to each sample. This data was hierarchically clustered using Pearson correlation and average linkage, resulting in two main clusters mainly explained by the presence or absence of Wnt signaling activation (Figure 3A). Cocktails exposing hiPSCs to CHIR clustered together and led to higher mesendoderm, endoderm and mesoderm scores, while conditions without CHIR clustered together and led to higher pluripotency and ectoderm scores. In addition, PCAs show that 91.3% of data variability (PC1) rely on Wnt signaling variation (Figure 3B). The exception was hiPSCs exposed to mTeSR1, which has LiCl (0.1 mM), a Wnt activator [42], and registered higher pluripotency and ectoderm scores, with lower mesendoderm, mesoderm and endoderm scores. These results seem to further highlight colony morphology observations: Wnt signaling activation was imposing hiPSCs to exit pluripotency and to commit towards mesendoderm lineages with or without FGF and TGF activation.

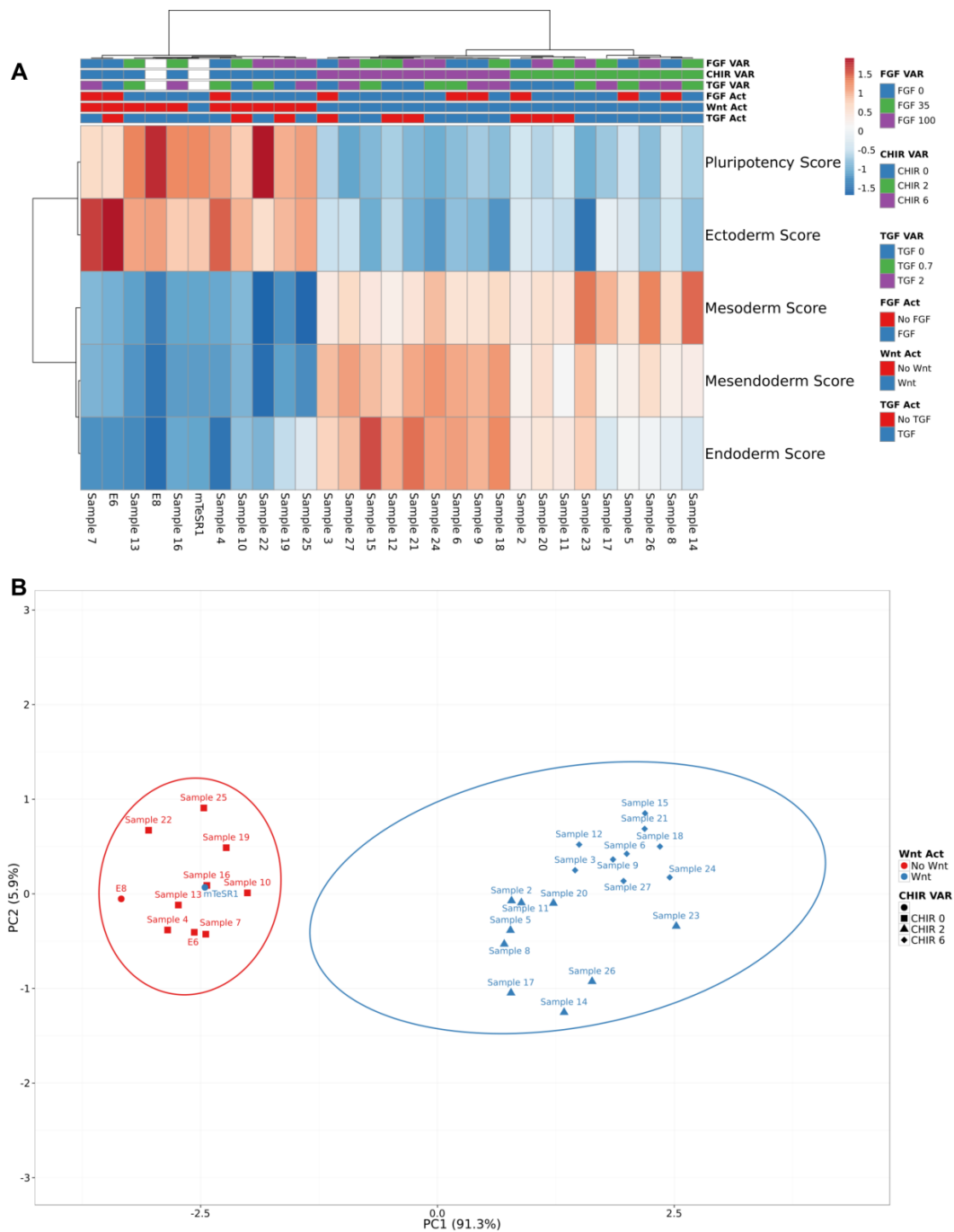


Figure 3. Hierarchical clustering and PCAs of full factorial design scores revealed two main clusters concordant with the presence or absence of CHIR. **(A)** Two main clusters were observed: Wnt activation, characterized by higher scores to mesendoderm lineages; and No Wnt activation, characterized by higher pluripotency and ectoderm scores. Clustering was performed using Pearson correlation and average linkage. Samples were labelled using signaling activation and no activation (FGF Act, Wnt Act and TGF Act; red and blue) and concentration variation (FGF VAR, CHIR VAR and TGF VAR; blue, green and purple). **(B)** The two main principal components together explained 97.2% of total data set variance. PC1 variance (91.3% of data set) corresponds to Wnt modulation. Only mTeSR1 clustered within the “No Wnt” group.

3.3. Full Quadratic Models for the Pluripotency and Ectoderm Lineage Scores

For visualizing the true impact of Wnt signaling in each score and discern if any synergies between signaling pathways were present, full quadratic models were fitted to the data, including quadratic, linear and two-way interactions. Contribution of each factor was considered statistically significant for p -values < 0.05 . As expected, CHIR supplementation contributed negatively for pluripotency scores (Figure 4A–C). Additionally, another significant contribution highlighted by the model could be observed, with synergy of FGF2 and CHIR contributing to lower pluripotency scores. Similar negative effects of CHIR supplementation were observed for ectoderm scores (Figure 4D–F). Furthermore, the FGF2 linear term and the TGF β quadratic term also contributed negatively to ectoderm scores. This result is in line with FGF2 showing to repress *PAX6* [16] and TGF inhibition facilitating neuroectoderm differentiation [55]. Contrarily, a synergy of FGF2 and CHIR contributed to higher ectoderm scores, which is coherent with reports showing that this synergy can lead to ectodermal neural crest and placode lineages [30].

To further explore the differences between ectoderm induction and pluripotency maintenance highlighted in our models, hiPSC were differentiated using a combination of dual SMAD inhibitors [55], ensuring inhibition of BMP and TGF β autocrine stimulation, and compared with cells differentiated in E6 medium only, therefore allowing hiPSCs to follow their inner circuitry and autocrine path [36]. Cells with no inhibitors (E6) showed similar profiles compared with neural differentiation induced with inhibitors (Dual), although showing a slight delay in the decrease of pluripotent markers *OCT4* and *NANOG*, and in the increase of *SOX1* (Figure 4G). This was reflected in *PAX6*⁺ cells originated at day 12 for all three cell lines tested, with dual SMAD inhibition resulting in a 20% to 40% increase in neural progenitors (Figure 4H,I). Nevertheless, cell differentiated in E6 medium only originated significant amounts of *PAX6*⁺ cells as well (Figure 4H). In fact, multiple neural rosettes were observed at day 12 for all the three hiPSC cell lines differentiated in E6 (Figure 4J), suggesting that this condition can allow a high degree of neural progenitor organization and commitment (Figure 4I) [36]. These results show the natural tendency for hiPSCs to converge to ectoderm if not actively stimulated [36,62], and are in line with the signaling inputs contributing significantly for both models.

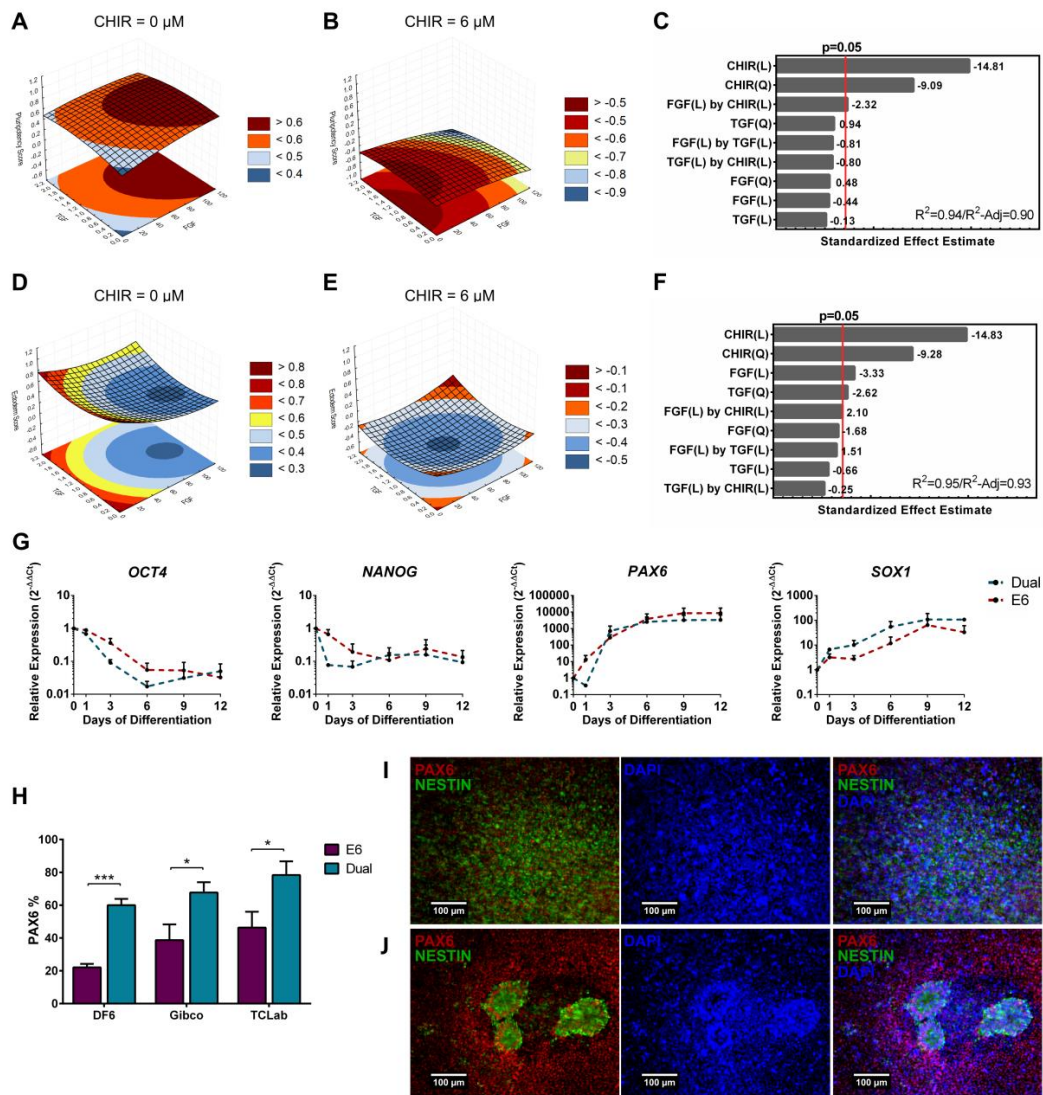


Figure 4. Quadratic models for the pluripotency and ectoderm scores highlighted a dominant negative contribution of Wnt signaling. (A,B) Representative curves of TGFβ and FGF2 contributions to pluripotency model with CHIR set at zero (A) and at 6 μM (B). Without CHIR, FGF2 high concentrations resulted in higher scores in the model, while with CHIR set at 6 μM, both TGFβ and FGF2 presence decreases pluripotency score. (C) CHIR linear and quadratic terms are the ones that contributed the most to the model, decreasing pluripotency scores. A statistically significant negative synergy can be seen between CHIR and FGF2. Model showed a good fit with a R^2 of 0.94 and a R^2 -Adjusted of 0.90. (D,E) Representative curves of TGFβ and FGF2 contributions to ectoderm model with CHIR set to zero (D) and to 6 μM (E). Without CHIR, the model output higher ectoderm scores, concordant with the significant negative effect. (F) Besides CHIR linear and quadratic negative effects, FGF2 linear, TGFβ quadratic and an interaction between CHIR and FGF2 contributed significantly to the model. FGF2 positively contributed when conjugated with CHIR, while negatively contributed for ectoderm score without CHIR. TGFβ negative quadratic term contribution can be clearly observed when FGF2 is zero (D) with higher ectoderm scores at full or no activation. Model showed a good fit to the data set with a R^2 of 0.95 and a R^2 -Adjusted of 0.93. (G) Real-time PCR comparison of E6 and dual SMAD inhibition neuroectoderm differentiation revealed a delayed expression decrease of the pluripotency markers *OCT4* and *NANOG* for the differentiation without factors (E6). Error bars, SEM, $n = 3$. (H) PAX6 positive cells quantification showed that dual SMAD differentiation originated 20% to 40% more PAX6⁺ cells for the three cell lines tested, when compared with E6 differentiation at day 12. Error bars, SEM, $n = 7$ DF6 and Gibco, and $n = 5$ TCLab. * p -value < 0.05, *** p -value < 0.001 (two-sided t -test). (I,J) At day 12, dual SMAD (I) differentiation did not result in neural rosette formation while cells differentiated using only E6 (J) consistently organized in neural rosettes throughout the culture. Scale bar: 100 μm. See Figures S2 and S3, and Tables S2 and S3 for pluripotency and ectoderm full model information.

3.4. Full Quadratic Models for the Mesendoderm and Mesoderm Lineage Scores

For the mesendoderm score model (Figure 5A–C), an inverse contribution from CHIR linear and quadratic terms was observed when compared with the pluripotency and ectoderm models, concordant with the results showed by the hierarchical clustering and PCAs. CHIR terms were the only components of the model that were statistically significant (Figure 5C). Input of 1/3 (2 μM) of CHIR registered a steep increase in mesendoderm scores with the full input doubling the score (Figure 5D). To further understand and validate the mesendoderm model, cardiac differentiation was performed using the full level of CHIR (6 μM) and compared with a low level of Wnt Activation (1 μM), since hiPSCs died in the differentiation conditions without CHIR. Only 6 μM of CHIR contributed significantly for the expression of the mesendoderm transcription factor T/Brachyury with a peak at day 1 of both protein (Figure 5E) and mRNA (Figure 5F), despite both conditions contributing similarly to a decrease in *OCT4* (Figure 5F). The observation that 1 μM of CHIR is insufficient for the entrance into mesendoderm is in full concordance with the model obtained, which predicts negative mesendoderm scores for that level of Wnt activation with or without the activation of TGF and FGF signaling (Figure S4).

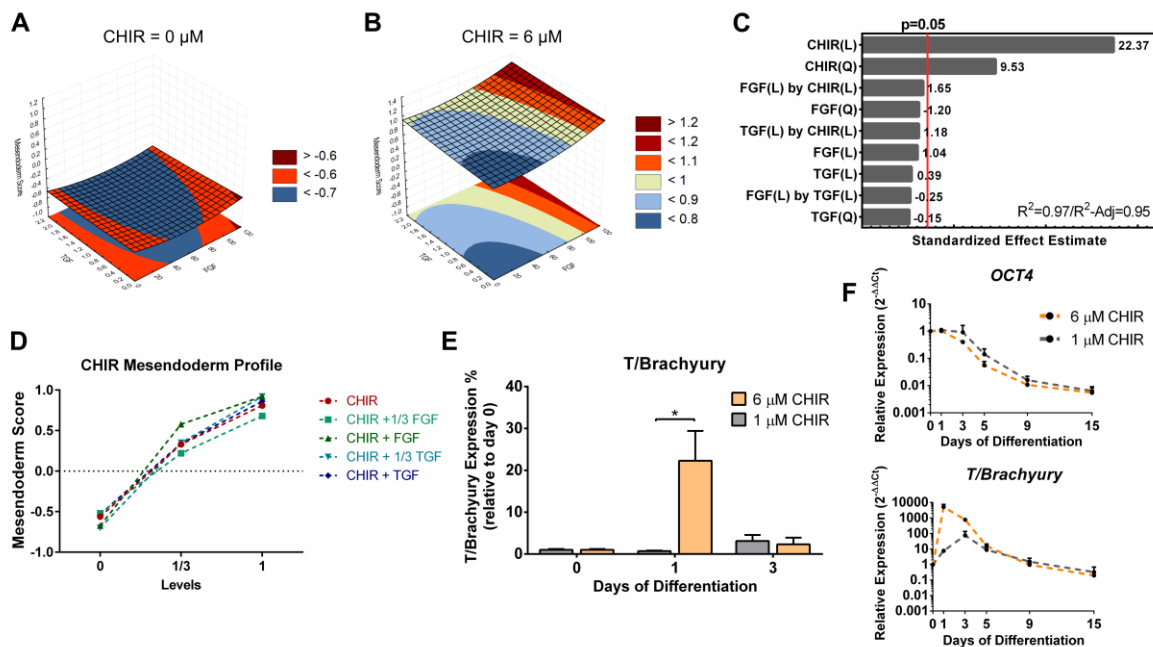


Figure 5. Quadratic model for the mesendoderm scores highlighted a strong positive contribution of Wnt signaling. (A,B) Representative curves of TGFβ and FGF2 contributions to the mesendoderm model with CHIR set to zero (A) and to 6 μM (B). (C) CHIR linear and quadratic terms of the model significantly contributed to the mesendoderm model. The model showed a very good fit to the data set, with a R² of 0.97 and a R²-Adjusted of 0.95. (D) Mesendoderm score profile of CHIR supplemented conditions shows an increase with CHIR concentration. (E) Flow cytometry of T/Brachyury showed that expression is significantly higher when 6 μM of CHIR is used compared to a lower activation level (1 μM). Error bars, SEM, n = 3. * p-value < 0.05 (two-sided t-test). (F) Real-time PCR comparison of *OCT4* and *T/Brachyury* for cardiac differentiation using 6 μM or 1 μM of CHIR showed a similar decreasing profile of *OCT4* gene expression, while 6 μM of CHIR contributed to a significantly higher gene expression of *T/Brachyury* at day 1. Error bars, SEM, n = 3. See Figure S4 and Table S4 for mesendoderm full model information.

Similarly, CHIR linear and quadratic terms also contributed significantly for the mesoderm score model (Figure 6A–C). In addition, FGF and CHIR linear terms present a positive synergy in the cutoff of statistical significance for the model (p = 0.06), which can be observed in Figure 6B.

This synergy is in agreement with reports showing that dual activation of FGF and Wnt promotes hiPSC differentiation into mesenchymal stem cells [63] and the generation of neuromesodermal progenitors [64,65]. FGF signaling also had a positive contribution for endoderm scores, with the FGF linear term and both CHIR quadratic and linear terms having a significant positive impact in the scores (Figures S6 and S7). This is in line with reports showing that both factors are essential to efficient definitive endoderm differentiation [31], and with FGF signaling pathway playing an important role in further differentiating the definitive endoderm, particularly into liver, lung and pancreatic lineages [18,59,66].

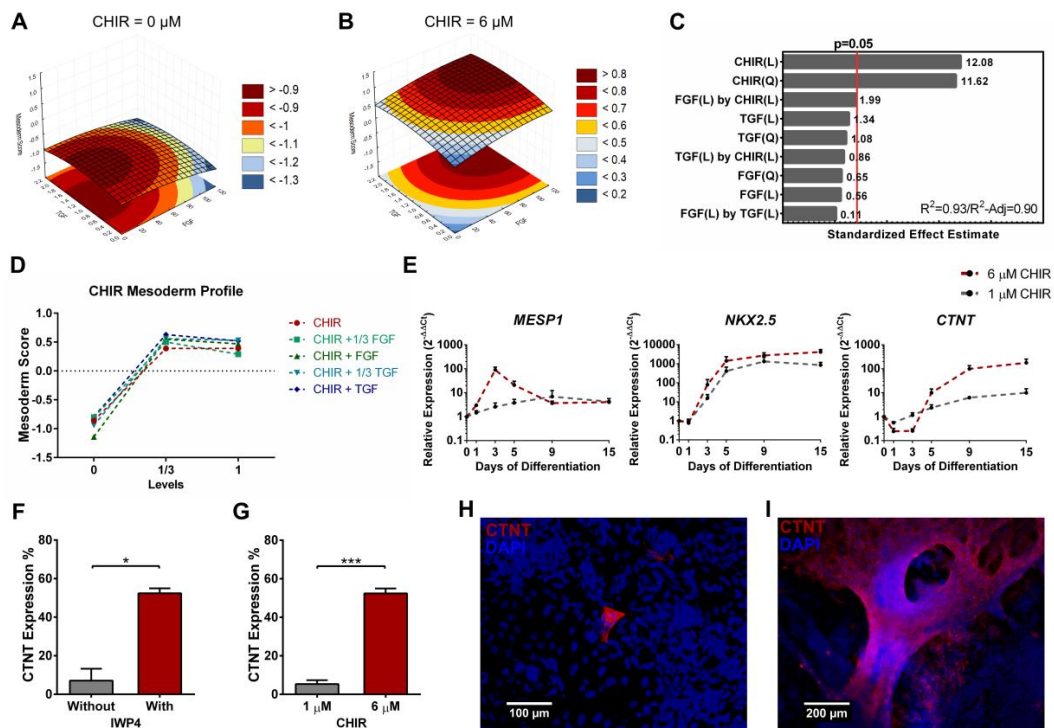


Figure 6. Quadratic model for the mesoderm scores highlighted the contribution of Wnt signaling with higher scores for intermediate CHIR concentrations. (A,B) Representative curves of TGFβ and FGF2 contributions to the mesoderm model with CHIR set at zero (A) and at 6 μM (B). (C) CHIR quadratic and linear terms significantly contributed to the mesoderm model. A synergy of CHIR with FGF can also be observed. Model showed a good fit to the data set with a R² of 0.93 and a R²-Adjusted of 0.90. (D) CHIR mesoderm profile shows an increase in mesoderm score at 1/3 activation, while higher concentrations maintain or slightly decrease mesoderm scores. (E) Real-time PCR comparison of cardiac differentiation using 6 μM or 1 μM of CHIR registered a higher gene expression of *MESP1*, with a peak at day 3, *NKX2.5* and *CTNT* when 6 μM is used. Error bars, SEM, n = 3. (F) Flow cytometry of cardiac differentiation with or without IWP4 showed that inhibiting Wnt signaling at day 3 is essential to efficiently obtain CTNT positive cells. Error bars, SEM, n = 3. * p-value < 0.05 (two-sided t-test). (G) Flow cytometry comparing Wnt signaling low or high activation levels showed that initial low activation originated few CTNT positive cells compared to 6 μM of CHIR. Error bars, SEM, n = 3. *** p-value < 0.001 (two-sided t-test). (H,I) Consistent with flow cytometry, immunostaining showed that 1 μM of CHIR (H, scale bar 100 μm) originated few cardiomyocytes while 6 μM originated cardiomyocytes throughout the culture (I, scale bar 200 μm). See Figure S5 and Table S5 for mesoderm full model information.

Contrarily to the mesendoderm model, stimulation with 2 μM of CHIR gave rise to the higher mesoderm scores, while the full input of 6 μM disclosed a tendency to stagnate or even decrease such scores (Figure 6D). For the generation of cardiac mesoderm, stimulation with 6 μM of CHIR resulted in increased *MESP1* expression, with a peak at day 3. Furthermore, *NKX2.5* expression was

not significantly affected by the level of Wnt signaling stimulation, but *CTNT* expression was one order of magnitude higher at 6 μM when compared with 1 μM of CHIR (Figure 6E). Concomitant with our model prediction, later inhibition of Wnt signaling, using IWP4 [27], was fundamental to obtain hiPSC-derived cardiomyocytes (Figure 6F), an observation that can be predicted in our model by the maintenance or even decrease in mesoderm scores when a full level input of CHIR was used (Figure 6D and Figure S5). Further aligned with the model predictions, low activation of Wnt signaling originated a low number of cardiomyocytes (Figure 6G), particularly sparse and rarely observable (Figure 6H) when compared to the full level of input (Figure 6I).

4. Discussion

There is a multitude of signaling pathways and interactions that govern pluripotency maintenance and lineage specification. Uncontrolled and poorly defined systems with increased noise to signal ratio hinder the ability to fully understand the independent and synergistic role of each factor in hPSC fate. The focus of our study was to develop a multiparameter approach to study the individual and synergistic effect of Wnt, FGF and TGF β signaling pathways using a dry-signaling culture system to avoid major unspecific signaling contributions. Our results showed that Wnt signaling had a dominant effect over FGF and TGF β inputs, pulling hiPSCs away from pluripotency and ectoderm, towards mesendoderm lineages. In addition, a synergy between FGF and Wnt signaling was observed, with a negative contribution to pluripotency scores and a positive contribution to ectoderm and mesoderm scores. FGF and TGF β signaling negatively contributed to ectoderm scores, which is connected with the well-known role of these signaling pathways in maintaining hiPSCs epiblast-like pluripotent state [4,15], and preventing cells to follow their inner circuitry towards neuroectoderm [36,62] (Figure 7).

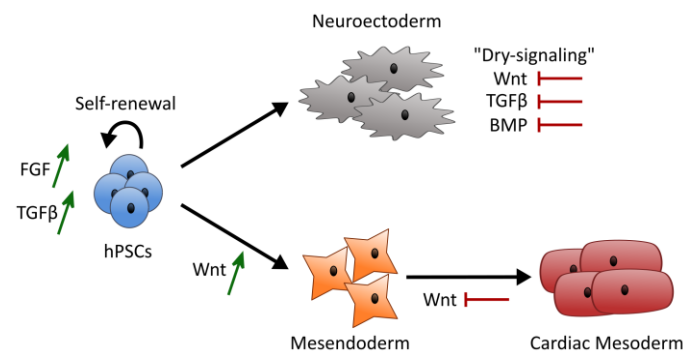


Figure 7. Model summarizing the overall results obtained using a dry-signaling multiparameter approach. Wnt signaling activation showed to be dominant over FGF and TGF β signaling driving hPSCs towards mesendoderm lineages. A synergy of FGF and CHIR was observed providing higher ectoderm scores or higher mesoderm scores and contributing to lower pluripotency scores. Contribution of FGF and TGF β signaling to maintain pluripotency scores seems to be connected with the negative contribution of both FGF and TGF β signaling to ectoderm scores, with absence of inputs inducing cells to follow their inner circuitry towards neuroectoderm.

In our model, the linear contribution of FGF and the quadratic term of TGF β show a negative correlation to the ectoderm score, with the lowest result obtained for levels of 100 ng/mL of FGF (full input) and 0.7 ng/mL of TGF β (1/3 of input). These values are in concordance with the level of input provided by both commercial media E8 and TeSR used to maintain hiPSCs pluripotency [15,42]. In addition, these levels of input prevent hiPSCs to naturally exit pluripotency towards neuroectoderm as observed by us and previously reported by Lippmann and coworkers [36], and are in concordance with reports showing that both factors inhibit neuroectoderm differentiation [16,55]. As suggested from our results, the role of FGF and TGF β in pluripotency maintenance seems to derive from a thin balance that prevents exit towards differentiation, instead of actively promoting and stimulating

pluripotency (Figure 4). This seems to be in line with the weak stability of the pluripotent epiblast-like state [7,8], and the bias of hPSCs towards neuroectoderm when only both factors are present to maintain pluripotency [36,62].

In the presence of Wnt signaling stimulation, TGF and FGF signaling effects were secondary, with all models showing CHIR terms as the most significant contributors. This dominance contributed negatively for pluripotency and ectoderm scores (Figure 4), and positively for mesendoderm, mesoderm and endoderm scores (Figures 5 and 6, Figures S5 and S6). These results are coherent with the literature and the well-known importance of Wnt signaling in the commitment of hPSCs towards mesendoderm and lineage specifications that rely on Wnt activation, such as cardiac mesoderm [27], pancreatic β -cells [67], mesenchymal stem cells [63], or epicardial lineage cells [29]. Besides contributing to commitment, Wnt signaling is described to have a role in promoting self-renewal and the naïve state of pluripotency [9–11,34]. Our pluripotency model predicted higher pluripotency scores for input levels lower than 2 μ M, but was unable to fully register a positive contribution of Wnt signaling to pluripotency. This might be explained by the epiblast-like state of the hiPSCs used in our study, and the inability of Wnt activation to reprogram cells to the naïve state by itself [10,11,49]. Once in a primed state, Wnt signaling role seems to transition from self-renewal to promoting further commitment to mesendoderm [23].

Synergies observed between Wnt signaling and FGF signaling in our models are also coherent with previously reported data. The positive contribution for the ectoderm model is in line with the role of FGF in repressing *PAX6* [16] and, together with Wnt, synergistically promoting the specification towards ectodermal neural crest and placode lineages [26,30]. The proximity between the pluripotent state with neuroectoderm specification can explain the negative synergistic impact of both pathways in the pluripotency model. In addition, contribution to lower pluripotency scores is also in line with the impact of Wnt in promoting mesendoderm lineages, and FGF being important to specify mesendoderm towards endoderm lineages, which is also coherent with the predictions of our endoderm model [18,31,59,66,68]. Lastly, the synergistic effect of both pathways in the mesoderm model is in line with the paraxial specification and direct differentiation of hiPSCs towards mesenchymal and neuromesodermal progenitors [32,63–65].

In conclusion, using a multifactorial, multiparameter modeling approach we predicted a dominant role of Wnt signaling over FGF and TGF signaling in our dry-signaling culture system. This modeling methodology also allowed the construction of models providing a rational understanding of hiPSCs pluripotency and commitment, allowing to discriminate the different synergies between FGF and Wnt signaling, in agreement with previously reported studies. Following this proposed framework, carefully designed 5-level fractional factorial designs coupled with multiple signaling activation dynamics should contribute to the construction of models with increased sensitivity and reduced variance and, consequently, providing an extra degree of comprehension of the complex regulatory system of human pluripotency and commitment.

Supplementary Materials: The following are available online at <http://www.mdpi.com/2306-5354/6/3/71/s1>, Table S1: Primer pairs used for real-time PCR, Table S2: ANOVA Pluripotency score model, Table S3: ANOVA Ectoderm score model, Table S4: ANOVA Mesendoderm score model, Table S5: ANOVA Mesoderm score model, Table S6: ANOVA Endoderm score model, Figure S1: Cell morphology changes during cocktail exposure, Figure S2: Full panel of the quadratic model for the pluripotency scores highlighting a dominant negative contribution of Wnt signaling, Figure S3: Full panel of the quadratic model for the ectoderm scores highlighting a dominant negative contribution of Wnt signaling with FGF signaling also contributing to lower ectoderm scores, Figure S4: Full panel of the quadratic model for the mesendoderm scores highlighting a strong and dominant contribution of Wnt signaling, Figure S5: Full panel of the quadratic model for the mesoderm scores highlighting the contribution of Wnt signaling with higher scores for intermediate CHIR concentrations, Figure S6: Full panel of the quadratic model for the endoderm scores highlighted the contribution of Wnt signaling with FGF signaling also positively contributing to higher endoderm scores, Figure S7: Endoderm Model Score profiles and Standardized Effect Estimate.

Author Contributions: Conceptualization, T.P.D., T.G.F., M.M.D. and J.M.S.C.; methodology, T.P.D.; investigation, T.P.D.; formal analysis, T.P.D.; visualization, T.P.D.; writing—original draft preparation, T.P.D.; writing—review and editing, T.G.F., M.M.D. and J.M.S.C.; supervision, T.G.F., M.M.D. and J.M.S.C.

Funding: Funding was received by iBB through Programa Operacional Regional de Lisboa 2020 (Project N. 007317), through the EU COMPETE Programme and from National Funds through FCT under the Programme grant (SAICTPAC/0019/2015, MITP-TB/ECE/0013/2013, UID/BIO/04565/2013 and PTDC/EMD-TLM/29728/2017), by the DISCOVERIES CTR from EU Teaming Phase2 (H2020-WIDESPREAD-01-2016-2017).

Acknowledgments: Tiago P. Dias acknowledge Fundação para a Ciência e a Tecnologia (FCT, Portugal, <http://www.fct.pt>) for financial support (SFRH/BD/78774/2011).

Conflicts of Interest: The authors declare no conflict of interest.

References

- Engle, S.J.; Puppala, D. Integrating human pluripotent stem cells into drug development. *Cell Stem Cell* **2013**, *12*, 669–677. [[CrossRef](#)]
- Merkle, F.T.; Eggan, K. Modeling human disease with pluripotent stem cells: From genome association to function. *Cell Stem Cell* **2013**, *12*, 656–668. [[CrossRef](#)] [[PubMed](#)]
- Fernandes, T.G.; Rodrigues, C.A.V.; Diogo, M.M.; Cabral, J.M.S. Stem cell bioprocessing for regenerative medicine. *J. Chem. Technol. Biotechnol.* **2014**, *89*, 34–47. [[CrossRef](#)]
- Ludwig, T.E.; Levenstein, M.E.; Jones, J.M.; Berggren, W.T.; Mitchen, E.R.; Frane, J.L.; Crandall, L.J.; Daigh, C.A.; Conard, K.R.; Piekarczyk, M.S.; et al. Derivation of human embryonic stem cells in defined conditions. *Nat. Biotechnol.* **2006**, *24*, 185–187. [[CrossRef](#)] [[PubMed](#)]
- Vallier, L.; Alexander, M.; Pedersen, R.A. Activin/Nodal and FGF pathways cooperate to maintain pluripotency of human embryonic stem cells. *J. Cell Sci.* **2005**, *118*, 4495–4509. [[CrossRef](#)] [[PubMed](#)]
- Wang, L.; Schulz, T.C.; Sherrer, E.S.; Dauphin, D.S.; Shin, S.; Nelson, A.M.; Ware, C.B.; Zhan, M.; Song, C.-Z.; Chen, X.; et al. Self-renewal of human embryonic stem cells requires insulin-like growth factor-1 receptor and ERBB2 receptor signaling. *Blood* **2007**, *110*, 4111–4119. [[CrossRef](#)] [[PubMed](#)]
- Kunath, T.; Saba-El-Leil, M.K.; Almousaillekh, M.; Wray, J.; Meloche, S.; Smith, A. FGF stimulation of the Erk1/2 signalling cascade triggers transition of pluripotent embryonic stem cells from self-renewal to lineage commitment. *Development* **2007**, *134*, 2895–2902. [[CrossRef](#)]
- Tesar, P.J.; Chenoweth, J.G.; Brook, F.A.; Davies, T.J.; Evans, E.P.; Mack, D.L.; Gardner, R.L.; McKay, R.D. New cell lines from mouse epiblast share defining features with human embryonic stem cells. *Nature* **2007**, *448*, 196–199. [[CrossRef](#)]
- Ying, Q.-L.; Wray, J.; Nichols, J.; Battle-Morera, L.; Doble, B.; Woodgett, J.; Cohen, P.; Smith, A. The ground state of embryonic stem cell self-renewal. *Nature* **2008**, *453*, 519–523. [[CrossRef](#)]
- Ware, C.B.; Nelson, A.M.; Mecham, B.; Hesson, J.; Zhou, W.; Jonlin, E.C.; Jimenez-Caliani, A.J.; Deng, X.; Cavanaugh, C.; Cook, S.; et al. Derivation of naive human embryonic stem cells. *Proc. Natl. Acad. Sci. USA* **2014**, *111*, 4484–4489. [[CrossRef](#)]
- Gafni, O.; Weinberger, L.; Mansour, A.A.; Manor, Y.S.; Chomsky, E.; Ben-Yosef, D.; Kalma, Y.; Viukov, S.; Maza, I.; Zviran, A.; et al. Derivation of novel human ground state naive pluripotent stem cells. *Nature* **2013**, *504*, 282–286. [[CrossRef](#)] [[PubMed](#)]
- Garcia-Maya, M.; Anderson, A.A.; Kendal, C.E.; Kenny, A.V.; Edwards-Ingram, L.C.; Holladay, A.; Saffell, J.L. Ligand concentration is a driver of divergent signaling and pleiotropic cellular responses to FGF. *J. Cell. Physiol.* **2006**, *206*, 386–393. [[CrossRef](#)] [[PubMed](#)]
- O’Leary, L.; Sevinç, K.; Papazoglou, I.M.; Tildy, B.; Detillieux, K.; Halayko, A.J.; Chung, K.F.; Perry, M.M. Airway smooth muscle inflammation is regulated by microRNA-145 in COPD. *Febs Lett.* **2016**, *590*, 1324–1334. [[CrossRef](#)] [[PubMed](#)]
- Blauwkamp, T.A.; Nigam, S.; Ardehali, R.; Weissman, I.L.; Nusse, R. Endogenous Wnt signalling in human embryonic stem cells generates an equilibrium of distinct lineage-specified progenitors. *Nat. Commun.* **2012**, *3*, 1070. [[CrossRef](#)] [[PubMed](#)]
- Chen, G.; Gulbranson, D.R.; Hou, Z.; Bolin, J.M.; Ruotti, V.; Probasco, M.D.; Smuga-Otto, K.; Howden, S.E.; Diol, N.R.; Propson, N.E.; et al. Chemically defined conditions for human iPSC derivation and culture. *Nat. Methods* **2011**, *8*, 424–429. [[CrossRef](#)] [[PubMed](#)]

16. Greber, B.; Coulon, P.; Zhang, M.; Moritz, S.; Frank, S.; Müller-Molina, A.J.; Araúzo-Bravo, M.J.; Han, D.W.; Pape, H.-C.; Schöler, H.R. FGF signalling inhibits neural induction in human embryonic stem cells. *EMBO J.* **2011**, *30*, 4874–4884. [[CrossRef](#)] [[PubMed](#)]
17. Xu, R.-H.; Sampsel-Barron, T.L.; Gu, F.; Root, S.; Peck, R.M.; Pan, G.; Yu, J.; Antosiewicz-Bourget, J.; Tian, S.; Stewart, R.; et al. NANOG Is a Direct Target of TGF β /Activin-Mediated SMAD Signaling in Human ESCs. *Cell Stem Cell* **2008**, *3*, 196–206. [[CrossRef](#)] [[PubMed](#)]
18. Teo, A.K.K.; Ali, Y.; Wong, K.Y.; Chipperfield, H.; Sadasivam, A.; Poobalan, Y.; Tan, E.K.; Wang, S.T.; Abraham, S.; Tsuneyoshi, N.; et al. Activin and BMP4 synergistically promote formation of definitive endoderm in human embryonic stem cells. *Stem Cells* **2012**, *30*, 631–642. [[CrossRef](#)] [[PubMed](#)]
19. Sato, N.; Meijer, L.; Skaltsounis, L.; Greengard, P.; Brivanlou, A.H. Maintenance of pluripotency in human and mouse embryonic stem cells through activation of Wnt signaling by a pharmacological GSK-3-specific inhibitor. *Nat. Med.* **2004**, *10*, 55–63. [[CrossRef](#)] [[PubMed](#)]
20. Ding, V.M.Y.; Ling, L.; Natarajan, S.; Yap, M.G.S.; Cool, S.M.; Choo, A.B.H. FGF-2 modulates Wnt signaling in undifferentiated hESC and iPS cells through activated PI3-K/GSK3 β signaling. *J. Cell. Physiol.* **2010**, *225*, 417–428. [[CrossRef](#)] [[PubMed](#)]
21. Cai, L.; Ye, Z.; Zhou, B.Y.; Mali, P.; Zhou, C.; Cheng, L. Promoting human embryonic stem cell renewal or differentiation by modulating Wnt signal and culture conditions. *Cell Res.* **2007**, *17*, 62–72. [[CrossRef](#)] [[PubMed](#)]
22. ten Berge, D.; Kurek, D.; Blauwkamp, T.; Koole, W.; Maas, A.; Eroglu, E.; Siu, R.K.; Nusse, R. Embryonic stem cells require Wnt proteins to prevent differentiation to epiblast stem cells. *Nat. Cell Biol.* **2011**, *13*, 1070–1075. [[CrossRef](#)] [[PubMed](#)]
23. Xu, Z.; Robitaille, A.M.; Berndt, J.D.; Davidson, K.C.; Fischer, K.A.; Mathieu, J.; Potter, J.C.; Ruohola-Baker, H.; Moon, R.T. Wnt/ β -catenin signaling promotes self-renewal and inhibits the primed state transition in naïve human embryonic stem cells. *Proc. Natl. Acad. Sci. USA* **2016**, *113*, E6382–E6390. [[CrossRef](#)] [[PubMed](#)]
24. Davidson, K.C.; Adams, A.M.; Goodson, J.M.; McDonald, C.E.; Potter, J.C.; Berndt, J.D.; Biechele, T.L.; Taylor, R.J.; Moon, R.T. Wnt/ β -catenin signaling promotes differentiation, not self-renewal, of human embryonic stem cells and is repressed by Oct4. *Proc. Natl. Acad. Sci. USA* **2012**, *109*, 4485–4490. [[CrossRef](#)] [[PubMed](#)]
25. Funayama, N.S.; Schachter, K.A.; Lerdrup, M.; Ekberg, J.; Hess, K.; Dietrich, N.; Honoré, C.; Hansen, K.; Semb, H. β -Catenin Regulates Primitive Streak Induction through Collaborative Interactions with SMAD2/SMAD3 and OCT4. *Cell Stem Cell* **2015**, *16*, 639–652. [[CrossRef](#)] [[PubMed](#)]
26. Menendez, L.; Yatskevich, T.A.; Antin, P.B.; Dalton, S. Wnt signaling and a Smad pathway blockade direct the differentiation of human pluripotent stem cells to multipotent neural crest cells. *Proc. Natl. Acad. Sci. USA* **2011**, *108*, 19240–19245. [[CrossRef](#)] [[PubMed](#)]
27. Lian, X.; Hsiao, C.; Wilson, G.; Zhu, K.; Hazeltine, L.B.; Azarin, S.M.; Raval, K.K.; Zhang, J.; Kamp, T.J.; Palecek, S.P. Robust cardiomyocyte differentiation from human pluripotent stem cells via temporal modulation of canonical Wnt signaling. *Proc. Natl. Acad. Sci. USA* **2012**, *109*, E1848–E1857. [[CrossRef](#)] [[PubMed](#)]
28. Dias, T.P.; Pinto, S.N.; Santos, J.I.; Fernandes, T.G.; Fernandes, F.; Diogo, M.M.; Prieto, M.; Cabral, J.M.S. Biophysical study of human induced Pluripotent Stem Cell-Derived cardiomyocyte structural maturation during long-term culture. *Biochem. Biophys. Res. Commun.* **2018**, *499*, 611–617. [[CrossRef](#)] [[PubMed](#)]
29. Bao, X.; Lian, X.; Qian, T.; Bhute, V.J.; Han, T.; Palecek, S.P. Directed differentiation and long-term maintenance of epicardial cells derived from human pluripotent stem cells under fully defined conditions. *Nat. Protoc.* **2017**, *12*, 1890–1900. [[CrossRef](#)] [[PubMed](#)]
30. Tchieu, J.; Zimmer, B.; Fattahi, F.; Amin, S.; Zeltner, N.; Chen, S.; Studer, L. A Modular Platform for Differentiation of Human PSCs into All Major Ectodermal Lineages. *Cell Stem Cell* **2017**, *21*, 399–410. [[CrossRef](#)]
31. Loh, K.M.; Ang, L.T.; Zhang, J.; Kumar, V.; Ang, J.; Auyeong, J.Q.; Lee, K.L.; Choo, S.H.; Lim, C.Y.Y.; Nichane, M.; et al. Efficient Endoderm Induction from Human Pluripotent Stem Cells by Logically Directing Signals Controlling Lineage Bifurcations. *Cell Stem Cell* **2014**, *14*, 237–252. [[CrossRef](#)] [[PubMed](#)]
32. Loh, K.M.M.; Chen, A.; Koh, P.W.W.; Deng, T.Z.Z.; Sinha, R.; Tsai, J.M.M.; Barkal, A.A.A.; Shen, K.Y.Y.; Jain, R.; Morganti, R.M.M.; et al. Mapping the Pairwise Choices Leading from Pluripotency to Human Bone, Heart, and Other Mesoderm Cell Types. *Cell* **2016**, *166*, 451–468. [[CrossRef](#)] [[PubMed](#)]

33. Singh, A.M.; Reynolds, D.; Cliff, T.; Ohtsuka, S.; Mattheyses, A.L.; Sun, Y.; Menendez, L.; Kulik, M.; Dalton, S. Signaling network crosstalk in human pluripotent cells: A Smad2/3-regulated switch that controls the balance between self-renewal and differentiation. *Cell Stem Cell* **2012**, *10*, 312–326. [[CrossRef](#)] [[PubMed](#)]
34. Barbosa, H.S.C.; Fernandes, T.G.; Dias, T.P.; Diogo, M.M.; Cabral, J.M.S. New Insights into the Mechanisms of Embryonic Stem Cell Self-Renewal under Hypoxia: A Multifactorial Analysis Approach. *PLoS ONE* **2012**, *7*, e38963. [[CrossRef](#)] [[PubMed](#)]
35. Lian, X.; Zhang, J.; Azarin, S.M.; Zhu, K.; Hazeltine, L.B.; Bao, X.; Hsiao, C.; Kamp, T.J.; Palecek, S.P. Directed cardiomyocyte differentiation from human pluripotent stem cells by modulating Wnt/ β -catenin signaling under fully defined conditions. *Nat. Protoc.* **2013**, *8*, 162–175. [[CrossRef](#)] [[PubMed](#)]
36. Lippmann, E.S.; Estevez-Silva, M.C.; Ashton, R.S. Defined human pluripotent stem cell culture enables highly efficient neuroepithelium derivation without small molecule inhibitors. *Stem Cells* **2013**, *32*, 1–18. [[CrossRef](#)] [[PubMed](#)]
37. Shi, Y.; Kirwan, P.; Livesey, F.J. Directed differentiation of human pluripotent stem cells to cerebral cortex neurons and neural networks. *Nat. Protoc.* **2012**, *7*, 1836–1846. [[CrossRef](#)]
38. Fernandes, T.G.; Duarte, S.T.; Ghazvini, M.; Gaspar, C.; Santos, D.C.; Porteira, A.R.; Rodrigues, G.M.C.; Haupt, S.; Rombo, D.M.; Armstrong, J.; et al. Neural commitment of human pluripotent stem cells under defined conditions recapitulates neural development and generates patient-specific neural cells. *Biotechnol. J.* **2015**, *10*, 1578–1588. [[CrossRef](#)]
39. Schindelin, J.; Arganda-Carreras, I.; Frise, E.; Kaynig, V.; Longair, M.; Pietzsch, T.; Preibisch, S.; Rueden, C.; Saalfeld, S.; Schmid, B.; et al. Fiji: An open-source platform for biological-image analysis. *Nat. Methods* **2012**, *9*, 676–682. [[CrossRef](#)]
40. Metsalu, T.; Vilo, J. ClustVis: a web tool for visualizing clustering of multivariate data using Principal Component Analysis and heatmap. *Nucleic Acids Res.* **2015**, *43*, W566–W570. [[CrossRef](#)]
41. Box, G.E.P.; Hunter, J.S.; Hunter, W.G. *Statistics for Experimenters: Design, Innovation, and Discovery*, 2nd ed.; Wiley-Interscience: Hoboken, NJ, USA, 2005; ISBN 978-0-471-71813-0.
42. Ludwig, T.E.; Bergendahl, V.; Levenstein, M.E.; Yu, J.; Probasco, M.D.; Thomson, J.A. Feeder-independent culture of human embryonic stem cells. *Nat. Methods* **2006**, *3*, 637–646. [[CrossRef](#)] [[PubMed](#)]
43. Beers, J.; Gulbranson, D.R.; George, N.; Siniscalchi, L.I.; Jones, J.; Thomson, J.A.; Chen, G. Passaging and colony expansion of human pluripotent stem cells by enzyme-free dissociation in chemically defined culture conditions. *Nat. Protoc.* **2012**, *7*, 2029–2040. [[CrossRef](#)] [[PubMed](#)]
44. Ring, D.B.; Johnson, K.W.; Henriksen, E.J.; Nuss, J.M.; Goff, D.; Kinnick, T.R.; Ma, S.T.; Reeder, J.W.; Samuels, I.; Slabiak, T.; et al. Selective Glycogen Synthase Kinase 3 Inhibitors Potentiate Insulin Activation of Glucose Transport and Utilization In Vitro and In Vivo. *Diabetes* **2003**, *52*, 588–595. [[CrossRef](#)] [[PubMed](#)]
45. Cline, G.W.; Johnson, K.; Regittig, W.; Perret, P.; Tozzo, E.; Xiao, L.; Damico, C.; Shulman, G.I. Effects of a novel glycogen synthase kinase-3 inhibitor on insulin-stimulated glucose metabolism in Zucker diabetic fatty (fa/fa) rats. *Diabetes* **2002**, *51*, 2903–2910. [[CrossRef](#)]
46. Cohen, P.; Goedert, M. GSK3 inhibitors: Development and therapeutic potential. *Nat. Rev. Drug Discov.* **2004**, *3*, 479–487. [[CrossRef](#)] [[PubMed](#)]
47. Bain, J.; Plater, L.; Elliott, M.; Shpiro, N.; Hastie, C.J.; Mclauchlan, H.; Klevernic, I.; Arthur, J.S.C.; Alessi, D.R.; Cohen, P. The selectivity of protein kinase inhibitors: A further update. *Biochem. J.* **2007**, *408*, 297–315. [[CrossRef](#)] [[PubMed](#)]
48. Chambers, S.M.; Mica, Y.; Lee, G.; Studer, L.; Tomishima, M.J. Dual-SMAD Inhibition/WNT Activation-Based Methods to Induce Neural Crest and Derivatives from Human Pluripotent Stem Cells. In *Human Embryonic Stem Cell Protocols. Methods in Molecular Biology*; Turksen, K., Ed.; Humana Press: New York, NY, USA, 2013; pp. 329–343.
49. Hanna, J.; Cheng, A.W.; Saha, K.; Kim, J.; Lengner, C.J.; Soldner, F.; Cassady, J.P.; Muffat, J.; Carey, B.W.; Jaenisch, R. Human embryonic stem cells with biological and epigenetic characteristics similar to those of mouse ESCs. *Proc. Natl. Acad. Sci. USA* **2010**, *107*, 9222–9227. [[CrossRef](#)] [[PubMed](#)]
50. Hammachi, F.; Morrison, G.M.; Sharov, A.A.; Livigni, A.; Narayan, S.; Papapetrou, E.P.; O'Malley, J.; Kaji, K.; Ko, M.S.H.; Ptashne, M.; et al. Transcriptional activation by Oct4 is sufficient for the maintenance and induction of pluripotency. *Cell Rep.* **2012**, *1*, 99–109. [[CrossRef](#)]
51. Nichols, J.; Smith, A. Naive and primed pluripotent states. *Cell Stem Cell* **2009**, *4*, 487–492. [[CrossRef](#)]

52. Chambers, I.; Colby, D.; Robertson, M.; Nichols, J.; Lee, S.; Tweedie, S.; Smith, A. Functional expression cloning of Nanog, a pluripotency sustaining factor in embryonic stem cells. *Cell* **2003**, *113*, 643–655. [[CrossRef](#)]
53. Silva, J.; Smith, A. Capturing pluripotency. *Cell* **2008**, *132*, 532–536. [[CrossRef](#)] [[PubMed](#)]
54. Noisa, P.; Ramasamy, T.S.; Lamont, F.R.; Yu, J.S.L.; Sheldon, M.J.; Russell, A.; Jin, X.; Cui, W. Identification and Characterisation of the Early Differentiating Cells in Neural Differentiation of Human Embryonic Stem Cells. *PLoS ONE* **2012**, *7*, e37129. [[CrossRef](#)] [[PubMed](#)]
55. Chambers, S.M.; Fasano, C.A.; Papapetrou, E.P.; Tomishima, M.; Sadelain, M.; Studer, L. Highly efficient neural conversion of human ES and iPS cells by dual inhibition of SMAD signaling. *Nat. Biotechnol.* **2009**, *27*, 275–280. [[CrossRef](#)] [[PubMed](#)]
56. Wang, L.; Chen, Y.-G. Signaling Control of Differentiation of Embryonic Stem Cells toward Mesendoderm. *J. Mol. Biol.* **2016**, *428*, 1409–1422. [[CrossRef](#)] [[PubMed](#)]
57. Xi, Q.; Wang, Z.; Zaromytidou, A.-I.; Zhang, X.H.-F.; Chow-Tsang, L.-F.; Liu, J.X.; Kim, H.; Barlas, A.; Manova-Todorova, K.; Kaartinen, V.; et al. A poised chromatin platform for TGF- β access to master regulators. *Cell* **2011**, *147*, 1511–1524. [[CrossRef](#)] [[PubMed](#)]
58. Hart, A.H.; Hartley, L.; Sourris, K.; Stadler, E.S.; Li, R.; Stanley, E.G.; Tam, P.P.L.; Elefanty, A.G.; Robb, L. Mixl1 is required for axial mesendoderm morphogenesis and patterning in the murine embryo. *Development* **2002**, *129*, 3597–3608.
59. Johannesson, M.; Ståhlberg, A.; Ameri, J.; Sand, F.W.; Norrman, K.; Semb, H. FGF4 and retinoic acid direct differentiation of hESCs into PDX1-expressing foregut endoderm in a time- and concentration-dependent manner. *PLoS ONE* **2009**, *4*, e4794. [[CrossRef](#)]
60. Chan, S.S.-K.; Shi, X.; Toyama, A.; Arpke, R.W.; Dandapat, A.; Iacovino, M.; Kang, J.; Le, G.; Hagen, H.R.; Garry, D.J.; et al. Mesp1 Patterns Mesoderm into Cardiac, Hematopoietic, or Skeletal Myogenic Progenitors in a Context-Dependent Manner. *Cell Stem Cell* **2013**, *12*, 587–601. [[CrossRef](#)]
61. Den Hartogh, S.C.; Schreurs, C.; Monshouwer-Kloots, J.J.; Davis, R.P.; Elliott, D.A.; Mummery, C.L.; Passier, R. Dual Reporter MESP1 mCherry/w -NKX2-5 eGFP/w hESCs Enable Studying Early Human Cardiac Differentiation. *Stem Cells* **2015**, *33*, 56–67. [[CrossRef](#)]
62. Nazareth, E.J.P.; Ostblom, J.E.E.; Lückner, P.B.; Shukla, S.; Alvarez, M.M.; Oh, S.K.W.; Yin, T.; Zandstra, P.W. High-throughput fingerprinting of human pluripotent stem cell fate responses and lineage bias. *Nat. Methods* **2013**, *10*, 1225–1231. [[CrossRef](#)]
63. Winston, T.S.; Suddhapas, K.; Wang, C.; Ramos, R.; Soman, P.; Ma, Z. Serum-Free Manufacturing of Mesenchymal Stem Cell Tissue Rings Using Human-Induced Pluripotent Stem Cells. *Stem Cells Int.* **2019**, *2019*, 1–11. [[CrossRef](#)] [[PubMed](#)]
64. Turner, D.A.; Hayward, P.C.; Baillie-Johnson, P.; Rue, P.; Broome, R.; Faunes, F.; Martinez Arias, A. Wnt/ β -catenin and FGF signalling direct the specification and maintenance of a neuromesodermal axial progenitor in ensembles of mouse embryonic stem cells. *Development* **2014**, *141*, 4243–4253. [[CrossRef](#)] [[PubMed](#)]
65. Gouti, M.; Tsakiridis, A.; Wymeersch, F.J.; Huang, Y.; Kleinjung, J.; Wilson, V.; Briscoe, J. In Vitro Generation of Neuromesodermal Progenitors Reveals Distinct Roles for Wnt Signalling in the Specification of Spinal Cord and Paraxial Mesoderm Identity. *Plos Biol.* **2014**, *12*, e1001937. [[CrossRef](#)] [[PubMed](#)]
66. Serls, A.E.; Doherty, S.; Parvatiyar, P.; Wells, J.M.; Deutsch, G.H. Different thresholds of fibroblast growth factors pattern the ventral foregut into liver and lung. *Development* **2005**, *132*, 35–47. [[CrossRef](#)] [[PubMed](#)]
67. Kunisada, Y.; Tsubooka-Yamazoe, N.; Shoji, M.; Hosoya, M. Small molecules induce efficient differentiation into insulin-producing cells from human induced pluripotent stem cells. *Stem Cell Res.* **2012**, *8*, 274–284. [[CrossRef](#)] [[PubMed](#)]
68. Hannan, N.R.F.; Segeritz, C.-P.; Touboul, T.; Vallier, L. Production of hepatocyte-like cells from human pluripotent stem cells. *Nat. Protoc.* **2013**, *8*, 430–437. [[CrossRef](#)] [[PubMed](#)]

